A hybrid method for MT-InSAR phase unwrapping for deformation monitoring in urban areas

Songbo Wu [a], Bochen Zhang [b], Xiaoli Ding [a,*], Naeem Shahzad [a], Lei Zhang [c], Zhong Lu [d]

[a] *Department of Land Surveying and Geo-Informatics and Research Institute for Land and Space, The Hong Kong Polytechnic University, Hung Hom, KLN 999077, Hong Kong, China*
[b] *MNR Key Laboratory for Geo-Environmental Monitoring of Great Bay Area, College of Civil and Transportation Engineering, Shenzhen University, 518060 Shenzhen, China*
[c] *College of Surveying and Geo-informatics, Tongji University, Shanghai 200000, China*
[d] *Roy M. Huffington Department of Earth Sciences, South Methodist University, Dallas, TX 75275, USA*

ABSTRACT

The accuracy of phase unwrapping in multi-temporal interferometric synthetic aperture radar (MT-InSAR) technology affect closely on the accuracy of ground deformation monitoring. In the urban area, urban infrastructures such as high-rise buildings present additional challenges to phase unwrapping due to the sudden elevation changes. The failure rate of phase unwrapping is often much higher in such areas, bringing more biases to the estimated deformation and height values. We propose a new method for MT-InSAR phase unwrapping especially for deformation monitoring in urban areas. The method isolates the propagation path of information by considering the building height information of a study area. Two quality controllers are also developed to refine the arc observation network structure for network adjustment and to correct the phase unwrapping errors. The proposed method is tested using both simulated and real datasets. The results show that the building height and the geolocation of the coherence points were estimated much more accurately, demonstrating the effectiveness of the proposed method in monitoring deformation of urban area.

1. Introduction

Urban areas often undergo various forms of ground deformation due to, e.g., underground construction (Wu et al. 2021), land reclamation (Wu et al. 2020), and infrastructure instability (Qin et al. 2021; Xiao et al. 2022). Monitoring such deformation is important to detect impending hazards. Multitemporal interferometric synthetic aperture radar (MT-InSAR), one of the most powerful geodetic techniques, has been developed to measure large-area high-resolution ground deformation since about 2000 (Berardino et al. 2002; Ferretti et al. 2001). In MT-InSAR applications, accurate deformation monitoring depends critically on the accuracy of phase unwrapping (Yu et al. 2019).

Several approaches have been developed for phase unwrapping in MT-InSAR. The first approach is the Permanent Scatterers InSAR (PS-InSAR) which analyses the point targets with high phase quality (Ferretti et al. 2001). Several variants of PS-InSAR methods have been subsequently developed by exploring e.g., 3D phase unwrapping (Hooper et al. 2004), and minimum cost flow (Pepe and Lanari 2006). The second approach makes use of homogeneous targets, (i.e., Distributed Scatterers), within a SAR stack to improve the phase quality to enhance phase unwrapping (Berardino et al. 2002; Ferretti et al. 2011; Jiang et al. 2015; Wang et al. 2022). Efforts have also been made on studying e.g., the deformation models (Van Leijen and Hanssen 2007), and networking strategies (Ojha et al. 2015) to enhance the accuracy of phase unwrapping in different application scenarios. However, in the urban area, the elevations of urban infrastructures vary suddenly and significantly, especially in the dense high-rise cities like Hong Kong, generating very high phase gradients in the interferograms that adversely affect the accuracy of phase unwrapping.

We propose a hybrid MT-InSAR method that will improve quality of phase unwrapping in applications in urban areas. To avoid the impact of discontinuous propagation paths, a height-guided networking strategy will be developed to constrain the propagation paths of the network solutions. To enhance the quality of phase unwrapping, two quality control strategies will also be developed to refine the spatial network structure and to correct the phase unwrapping errors.
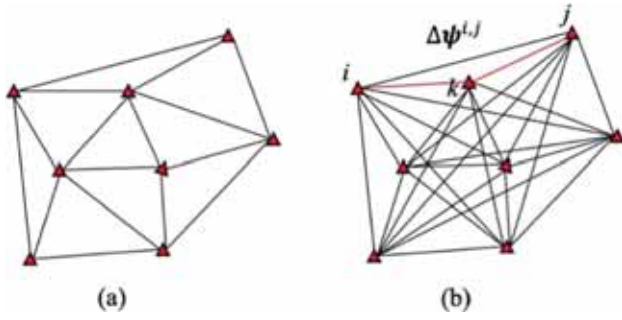

Fig. 1. Spatial network formed by (a) Delaunay triangulation, (b) freely connected network. Each line is a double differential observation between a point pair, or an arc as called commonly.

2. MT-InSAR phase unwrapping

Let us assume $N + 1$ co-registered SAR images are obtained to generate M interferograms (IFGs) using either a single or multiple master interferometric network. P coherent points are selected from the IFGs stack based on a phase quality threshold. A Delaunay triangulation network (Fig. 1(a)) or other networks such as the freely connected network (FCN) (Fig. 1(b)) can be formed to link the selected points. Double differenced phase between point pairs (i.e., arcs) in all the IFGs (e.g., the arc between point i and j in Fig. 1(b)) are taken as the observations. The double differenced phase on an arc is expressed as (Ferretti et al. 2001),

$$\Delta\psi^{i,j} = wrap\left\{\Delta\phi_{defo}^{i,j} + \Delta\phi_{topo}^{i,j} + \Delta\phi_{orb}^{i,j} + \Delta\phi_{APS}^{i,j} + \Delta\phi_{noise}^{i,j}\right\} \quad (1)$$

where $wrap\{\bullet\}$ represents the wrapping operation; $\Delta\psi^{i,j}$ is the wrapped double differenced phase; $\Delta\phi_{defo}^{i,j}$ is the deformation phase; $\Delta\phi_{topo}^{i,j}$ is the topographic residual phase (DEM error); $\Delta\phi_{orb}^{i,j}$ and $\Delta\phi_{APS}^{i,j}$ are phase components induced by the satellite orbital error and the atmospheric delays, respectively; $\Delta\phi_{noise}^{i,j}$ is the decorrelation noise. $\Delta\phi_{orb}^{i,j}$ can be compensated by, e.g., estimating the orbital errors (Zhang et al. 2014). $\Delta\phi_{APS}^{i,j}$ can be mitigated to certain extent by spatiotemporal filtering. For urban areas, since the arcs are constructed with high coherent points and are typically short (say $distance < 1km$), it is not significantly affected by the decorrelation and atmospheric effects (Hanssen 2001). Therefore, the first and second items are considered as the main phase components (MPC) of an arc. Therefore, Equation (1) can be written as,

$$\Delta\psi^{i,j} = wrap\left\{\frac{4\pi}{\lambda}\Delta d^{i,j} + \frac{4\pi \mathbf{B}}{\lambda\rho\sin\vartheta}\Delta h^{i,j} + \Delta\phi_{res}^{i,j}\right\} \quad (2)$$

where $\Delta d^{i,j}$ and $\Delta h^{i,j}$ represent the unknown deformation and DEM error. In general, $\Delta d^{i,j}$ is parameterized with the deformation model i.e., $\Delta d^{i,j} = \Delta \mathbf{t} \bullet \Delta v^{i,j}$. $\mathbf{B}$, ρ, λ and ϑ are the perpendicular baseline of the IFG, slant-range between radar sensor and the target, radar wavelength, and incidence angle, respectively. MPC is estimated using the periodogram solver by a discrete search of $\Delta v^{i,j}$ and $\Delta h^{i,j}$ in given intervals to maximize the arc quality, e.g., using temporal phase coherence (TPC) that is calculated by (Ferretti et al. 2001; Pepe et al. 2011),

$$\arg\max_{\Delta v^{i,j},\Delta h^{i,j}}\left\{\widehat{\gamma} = \frac{1}{M}\left|\sum_{k=1}^{M}\Delta\phi_{k,res}^{i,j}\right|\right\}, \quad (3)$$

$$with\ \Delta\phi_{k,res}^{i,j} = e^{j\Delta\psi_k^{i,j}}\ e^{-j\left(\frac{4\pi}{\lambda}\Delta t_k \cdot \Delta v^{i,j} + \frac{4\pi \mathbf{B}_k^{i,j}}{\lambda\rho\sin\vartheta}\Delta h^{i,j}\right)}$$

where $\widehat{\gamma}$ represents the TPC. A larger value of $\widehat{\gamma}$ implies a better estimation of the MPC. The parameters of $\Delta v^{i,j}$ and $\Delta h^{i,j}$ are normally considered to be estimated correctly when $\widehat{\gamma} > 0.7$. After all the arcs are estimated, a spatial network adjustment can be carried out to determine the parameters and the unwrapped phase by assuming that the phase residuals $\Delta\phi_{res}^{i,j} \in (-\pi, \pi]$ (Ferretti et al. 2001). The deformation time series is retrieved with the spatiotemporal filtering or with a predefined deformation model in the process referred to as post-processing (Chang and Hanssen 2015).

Many factors affect the accuracy of phase unwrapping discussed above. First, the network-based unwrapping algorithms are path dependent and can potentially diverge. For example, an arc that connects a point on a building to a point on the road can bias the estimation of the building height (Fig. 2(a)) compared with the results from the correct propagation path in Fig. 2(b). Second, dense double-differenced observations are often used (Wu et al. 2019). Such dense observations generate the solutions with different qualities that can propagate the errors during the spatial network adjustment. Therefore, a high-quality network needs to be extracted before the network adjustment (Jiang and Guarnieri 2020). Finally, current quality indicators of arc solutions (e.g., temporal coherence) only indicate the temporal variation of the residual phase, the arcs with large residual can generate the phase ambiguity during the adjustment. Therefore, phase unwrapping errors are often unavoidable.
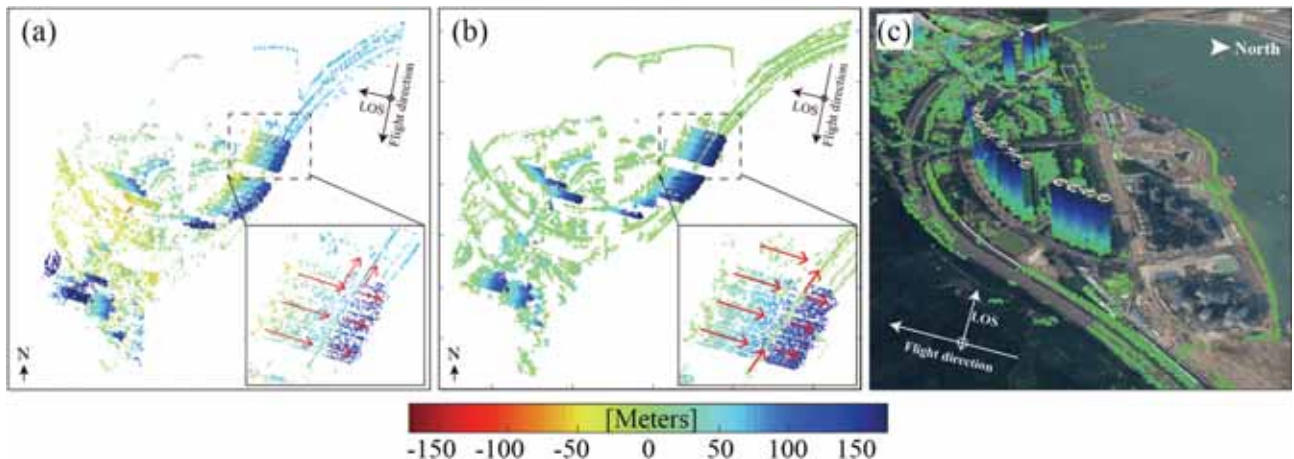
Fig. 2. Estimated building height with (a) a low-quality integration path and (b) a correct path. (c) Overlay the points on Google Earth 3D-model. The red arrows indicate the integration path of network adjustment.
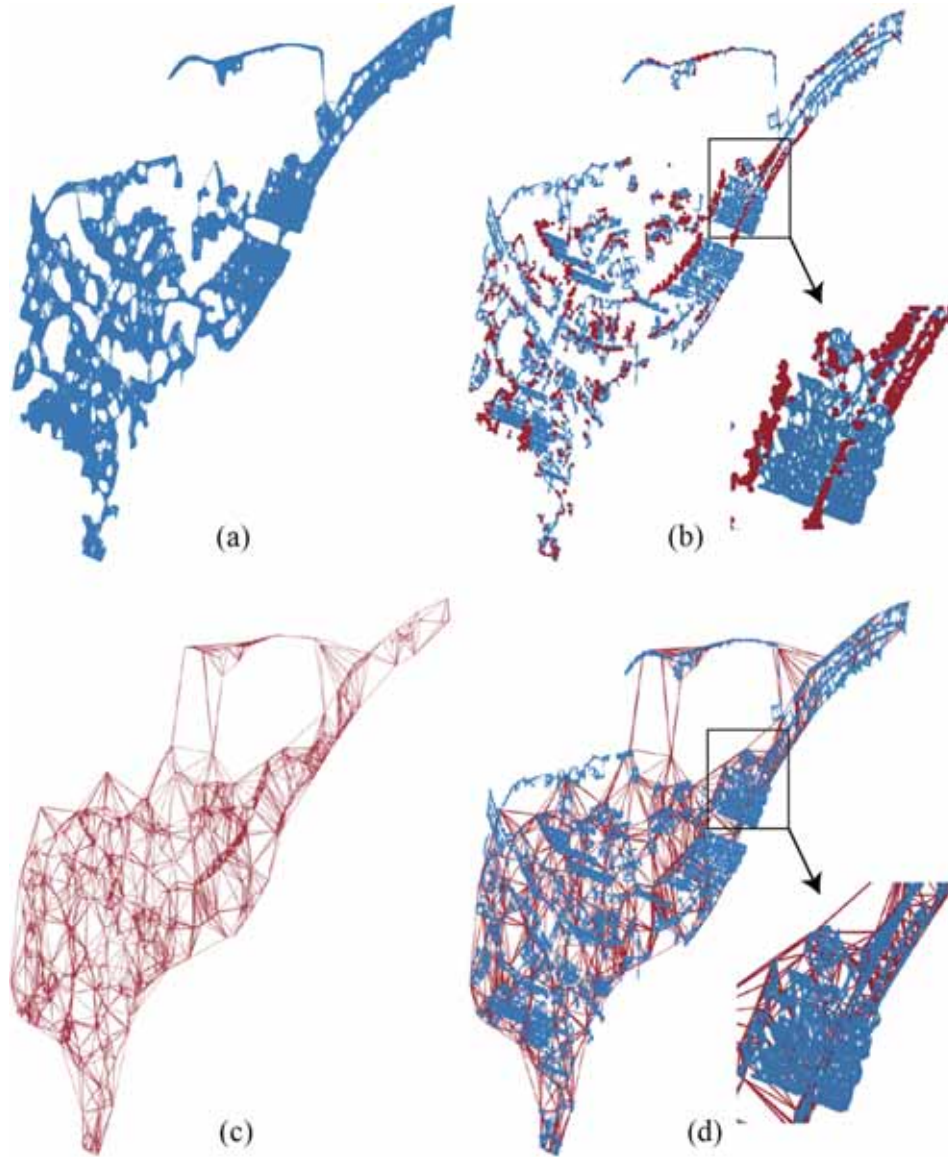
Fig. 3. (a) LFCN, (b) subset networks due to removal of arcs with large height differences, (c) constrained network, and (d) network merging (b) and (c). The red dots in (b) are the selected constraint points.
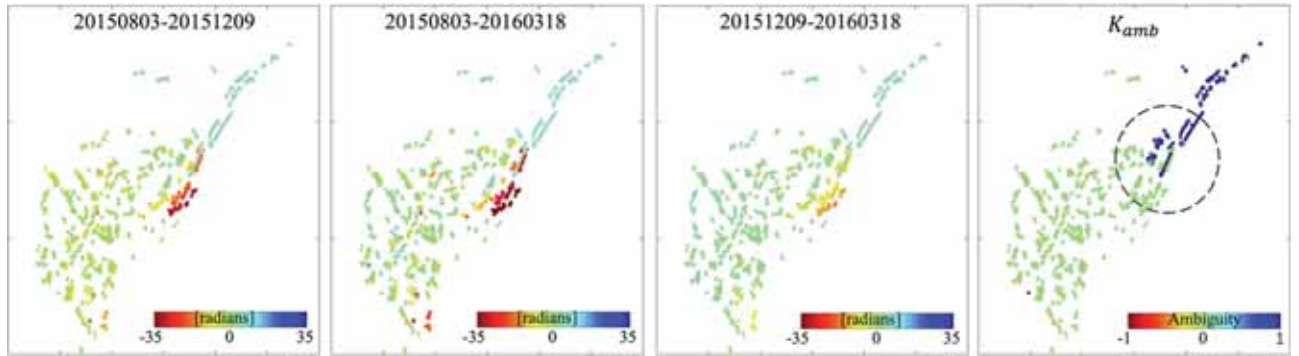
Fig. 4. Closure phase of an interferometric triplets. The black circle indicates where the unwrapping error occurred.

3. Methodology

A height-guided spatial networking strategy and two quality control strategies (i.e., spatial network refinement and unwrapping error correction) are proposed to enhance the quality of MT-InSAR phase unwrapping in urban areas.
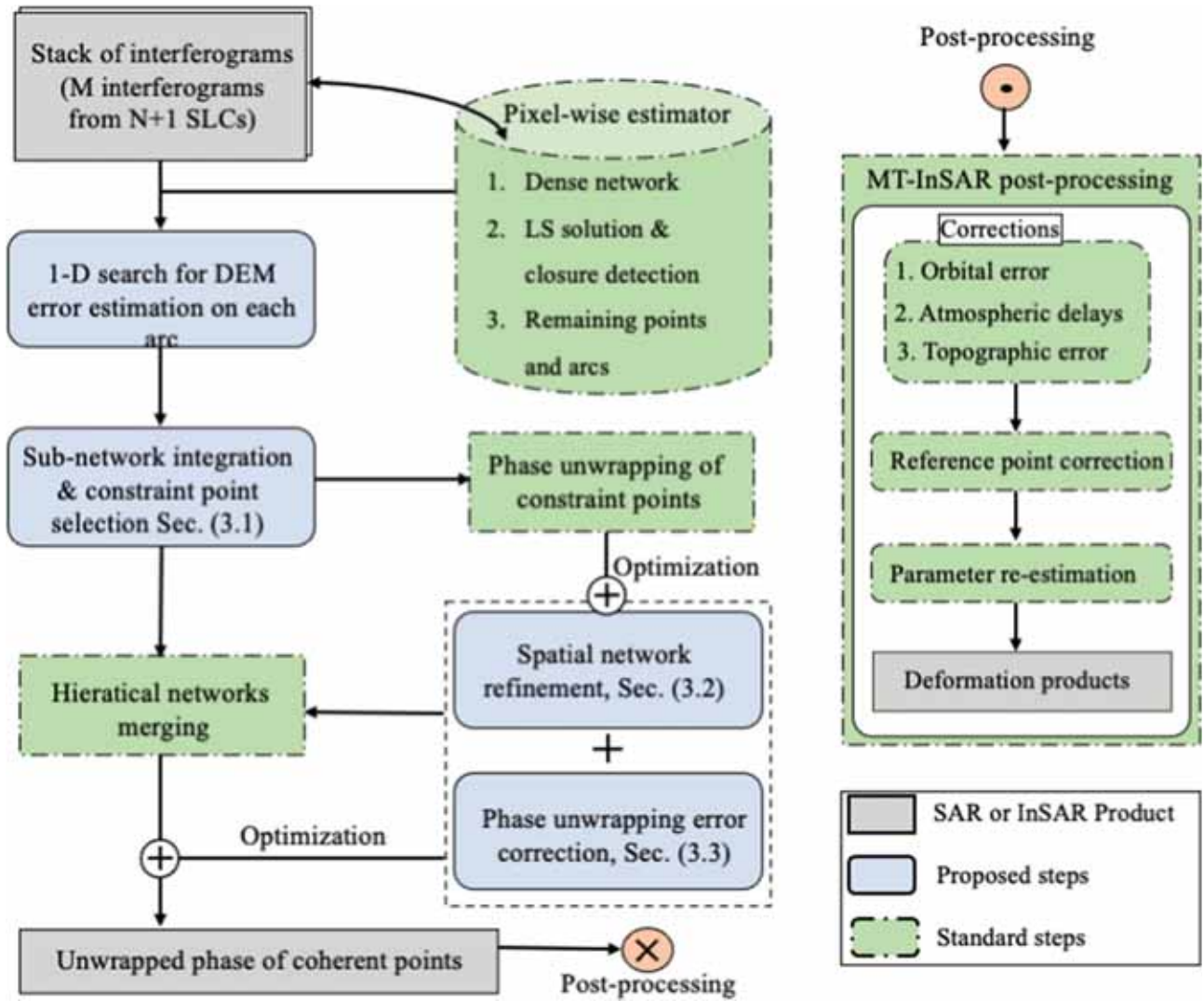
Fig. 5. Flow chart of the proposed method.

3.1. Height-guided networking

A height-guided spatial networking (HgN) strategy is proposed to select the proper arcs that are used to propagate the solutions between the points to mitigate the impact of elevation discontinuities. More specifically, we perform a discrete search of Δh for each arc constructed by a spatial network, e.g., Fig. 3(a) generated by the Pixelwise estimator (Wu et al. 2019) with the local freely connected network (LFCN),

$$\underset{\Delta h^{i,j}}{\mathrm{argmax}}\left\{\widehat{\gamma}=\frac{1}{M}\left|\sum_{k=1}^{M}\Delta\phi_{res}^{i,j}\right|\right\},\ with \Delta\phi_{res}^{i,j}=e^{j\Delta\psi_{k}^{i,j}}e^{-j\left(\frac{4\pi B_{k}^{i,j}}{\lambda\rho sin\theta}\Delta h^{i,j}\right)} \qquad (4)$$

where $\widehat{\gamma}$ represents the TPC. The arcs with smaller height differences are kept while the others are removed. The threshold setting for the arc solution is experience value, e.g., $\left|\Delta h^{i,j}\right|\left\langle 60\&\widehat{\gamma}>0.7\right.$. Spatially isolated *subnetworks* may be generated in this process (e.g., Fig. 3(b)). In this case, the point heights can be estimated through network adjustment within each subnetwork. The points with lower height within each subnetwork can be selected as the constraint point (CP) (e.g., the red dots in Fig. 3(b)). Then the unwrapped phase of CPs is retrieved and used to generate a constrained network with DTN (Fig. 3(c)). Finally, the subnetworks and the constrained network are merged to propagate the solutions between the subnetworks and to construct a height-guided

spatial network (Fig. 3(d)) for a final network adjustment. The height-guided networking is verified in Section 4.1.

3.2. Spatial network refinement

Since the quality of the arc solutions is important for the subsequent network adjustment, the arc solutions with high-quality can be extracted from the redundant arcs according to their qualities (Jiang and Guarnieri 2020). For example, in Fig. 1(b), if the quality of arc (i, j) is low, we can use the other two arcs in red to propagate the solutions from point i to point j ($i{\rightarrow}k{\rightarrow}j$). We here define the redundant arc solutions as set **R** and the selected arc solutions as set **S**, where $\mathbf{S}\in\mathbf{R}\&\mathbf{S}_{qualities}>\mathbf{R}_{qualities}$. Specifically, a Delaunay network is constructed as the reference network structure to connect all the points. For each arc of the Delaunay network, we applied the shortest path algorithm (Jianya 1999) to find the optimal arc paths from the redundant network, **R**, generated by LFCN to replace this arc. Accordingly, when all the arcs have been replaced, the refined set **S** is extracted.

To define a weight function for the shortest path algorithm, the *temporal closure values* (TCV) of the phase residuals is calculated for each arc in set **R**. According to (Pepe and Lanari 2006), the smaller the TCV is, the less phase ambiguities exists in the arc. We calculated the TCV using Equation (5) to ensure that the arcs with less TCV have smaller positive weights.
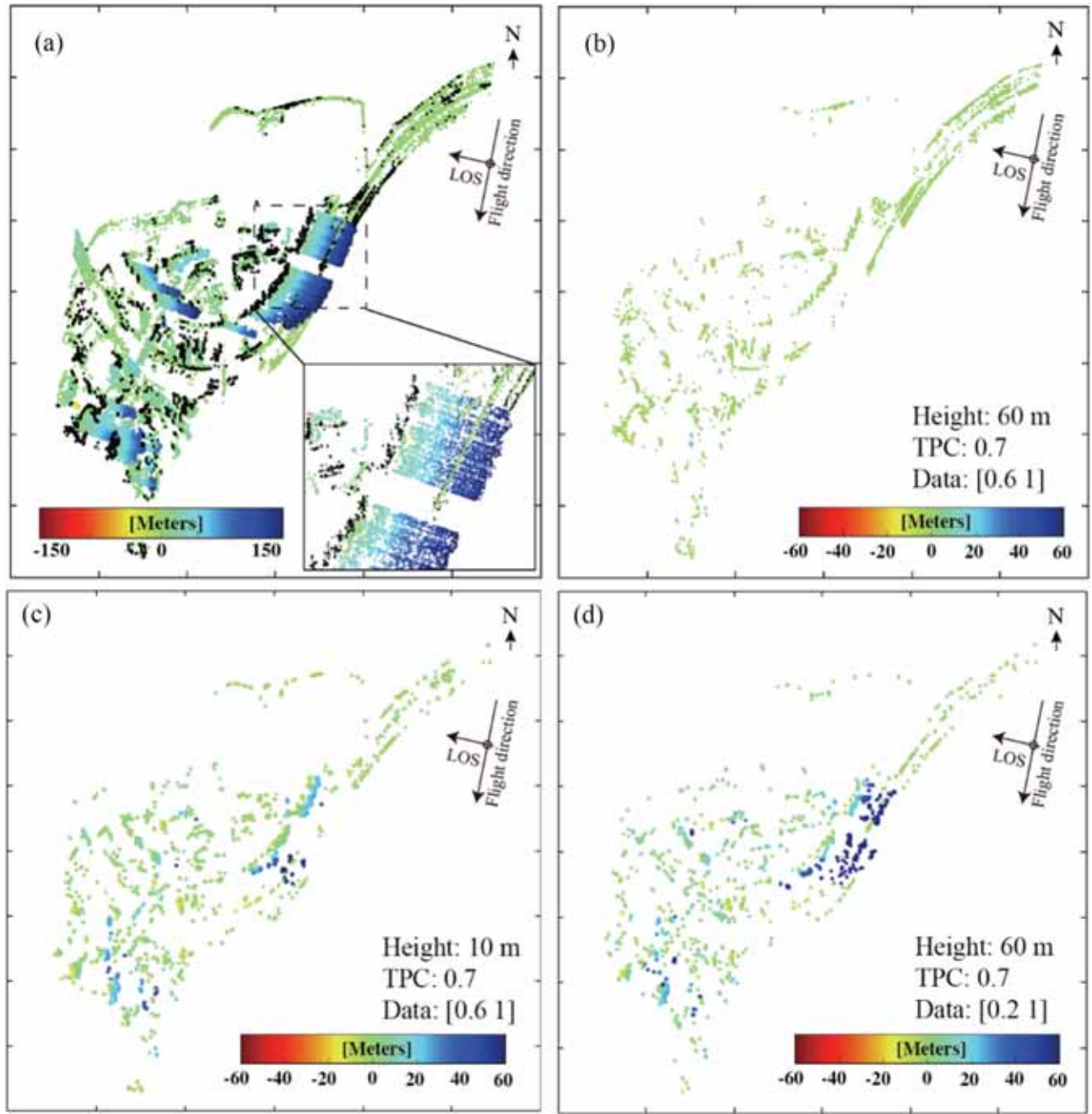
Fig. 6. "Real" height of (a) all coherent points used in the simulation and (b) selected CPs. The black dots in (a) are the locations of the CPs in (b).

$$C = \sum_{n=1}^{T} \left(\left| \Delta\phi_{res}^{a,b} + \Delta\phi_{res}^{b,c} - \Delta\phi_{res}^{a,c} \right| \right)_n \tag{5}$$

where C represents the sum of the TCV in an arc; T is the number of network triplets in the interferometric network. $\Delta\phi_{res}^{a,b}$ represents the phase residuals between the unwrapped and original wrapped phase of an arc; a, b and c represent three SAR acquisitions. The accuracy of the spatial network adjustment is then improved when the refined network is used. The effectiveness of spatial network refinement (SnR) strategy will be verified in Section 4.2.

3.3. Correction of phase unwrapping error

After achieving the unwrapped phase, the TCV has been used to identify phase jumps (Agram and Simons 2015). The TCV and ambiguity

index (K_{amb}) of one pixel in a network triplet is calculated by,

$$\phi_{Triplet} = \Delta\phi^{a,b} + \Delta\phi^{b,c} - \Delta\phi^{a,c}$$

$$K_{amb} = round\left[(\phi_{Triplet} - wrap(\phi_{Triplet}))/2\pi \right] \tag{6}$$

where $\Delta\phi^{a,b}$ represents the unwrapped phase from SAR acquisitions a and b. $round[\bullet]$ stands for the nearest integer number. $\phi_{Triplet}$ represents the TCV of the unwrapped phase that should not have phase ambiguity ($K_{amb} = 0$). Fig. 4 gives an example of phase unwrapping error.

To identify the source of phase unwrapping errors, each IFG that acts the vertex of a network triplet must be inspected. One network triplet can only indicate the pixel that has phase unwrapping error in one or more of the three IFGs used to calculate the triplet. With the help of multiple network triplets from multiple master interferometric network may make it possible to correct the phase unwrapping error (Hussain
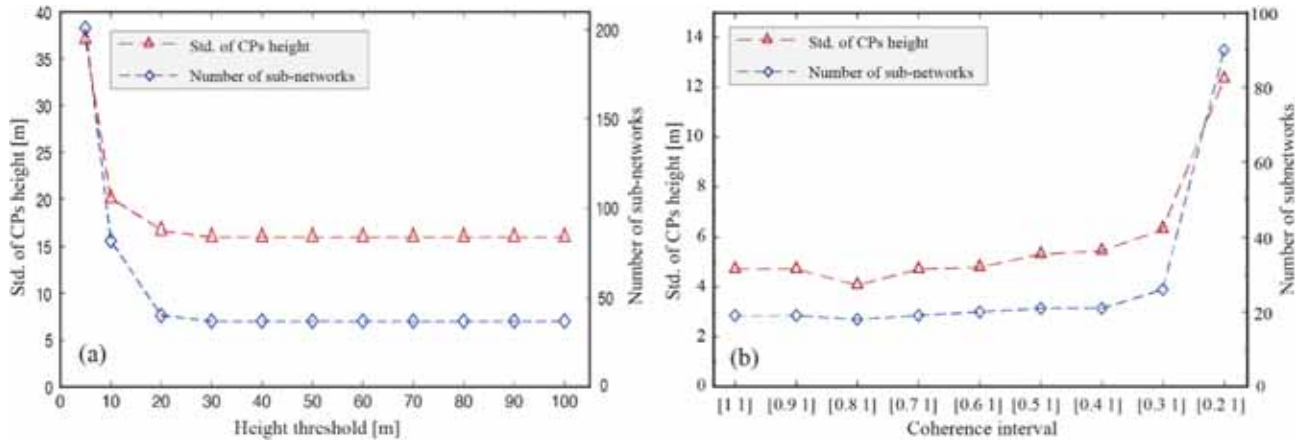
Fig. 7. The statistical results of the CPs height and subnetworks numbers using different height thresholds and phase quality.
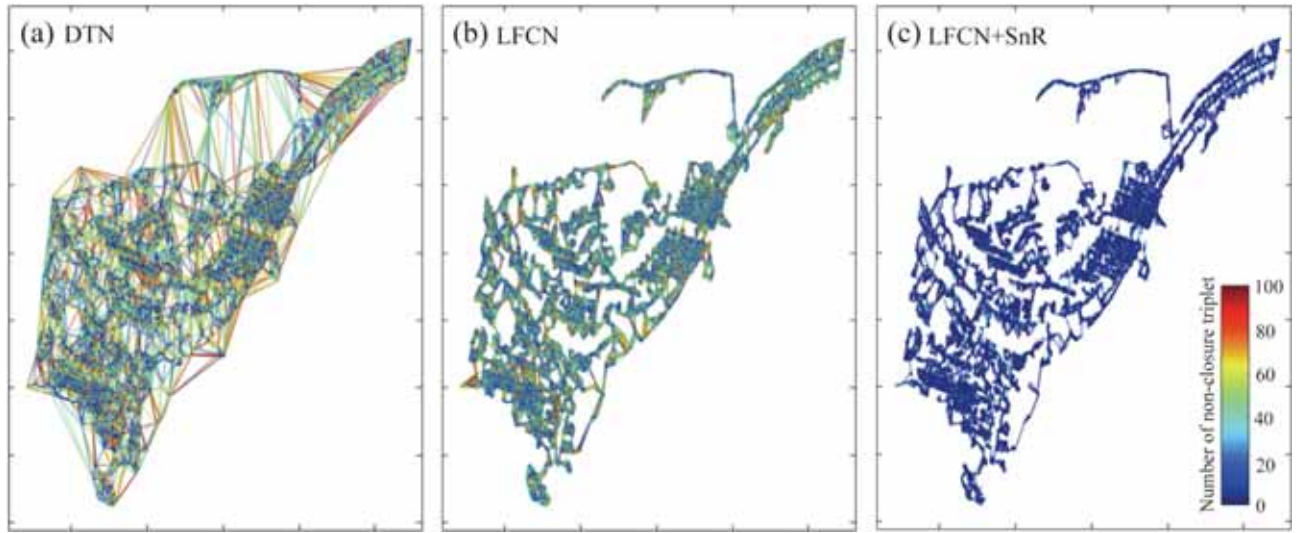

Fig. 8. TCV of network triplets in (a) DTN, (b) LFCN with closure detection, and (c) LFCN with SnR using the simulated observations in coherence interval [0.7 1].
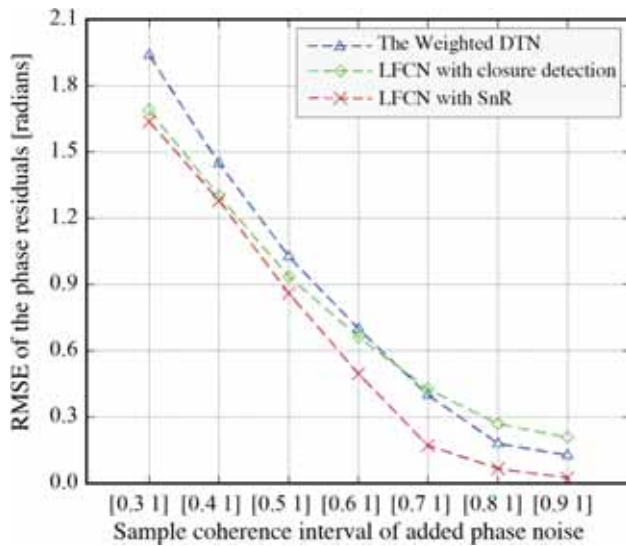

Fig. 9. RMSE between simulated and unwrapped phase from weighted DTN (in blue), LFCN with closure detection (in green), and LFCN with SnR (in red).
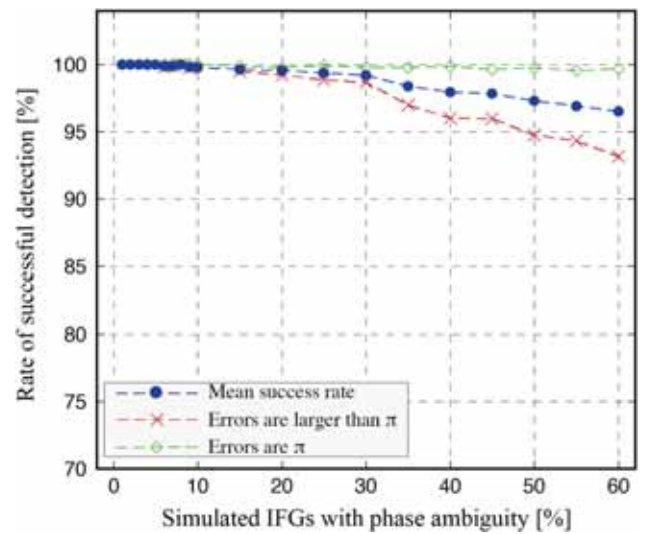
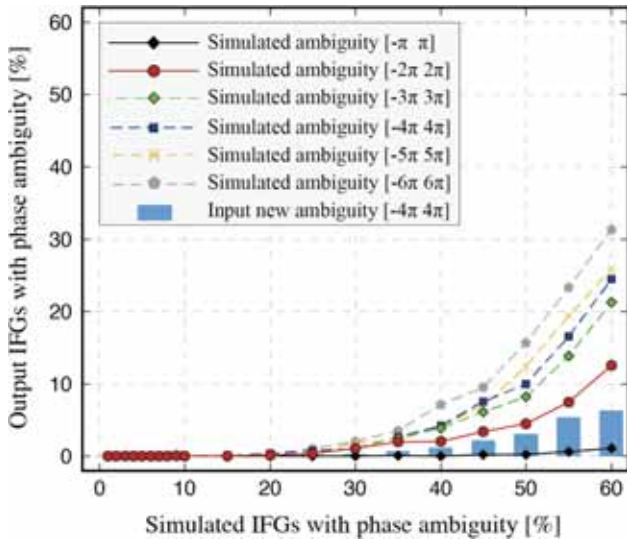**Fig. 10.** Success rate of unwrapping error detection.

Fig. 11. Rate of successful unwrapping error correction.

et al. 2016; Yang et al. 2013; Zhang et al. 2019). The correction of the unwrapping errors of a pixel can be obtained by,

$$\widehat{K}_{amb} = argmin \|\mathbf{L}_{Triplet} \bullet K_{amb} + \frac{\phi_{Triplet} - wrap(\phi_{Triplet})}{2\pi}\|_2 + \alpha\|K_{amb}\|_1 \quad (7)$$

where $\mathbf{L}_{Triplet}$ is $T \times M$ matrix; T and M are the number of network triplets and the number of the IFGs, respectively. Each row of $\mathbf{L}_{Triplet}$ corresponds to a network triplet while a column consists of 1 or -1 when the IFG is a member of a triplet or 0 otherwise. K_{amb} is the unknown integer phase ambiguity. As each IFG has an unknown K_{amb}, the design matrix $\mathbf{L}_{Triplet}$ can be rank deficient, may not always have a unique solution. Therefore, regularization is needed, such as apply the L^1-norm regularized least squares optimization in Equation (7), where α is the

parameter to trade-off between the L^1 and L^2-norm regulation (Zhang et al. 2019).

The rank deficiency problem of $\mathbf{L}_{Triplet}$ can be avoided if the IFGs with ambiguities are identified correctly. We propose to use the residual phase to identify specific IFGs with ambiguities. The phase residual between original wrapped and unwrapped phase, $\Delta\psi_{res}$, is used to identify IFG with unwrapping error that locates in $(-\pi, \pi]$. Before this procedure, the phase correction of the reference point should be carried out (Chang 2015), which has been introduced in Supplementary Material. In addition, because of the IFGs with significant unwrapping error will lead to large phase residual during least-squares (LS) inversion (Zhang et al. 2011), we also use the phase residual of the LS estimation of the successive interval phase ($\Delta\phi_{suc}$) using unwrapped IFGs to identify the IFG with modulo 2π unwrapping error. Two types of phase residuals can be calculated by,

$$\begin{cases} \Delta\psi_{res} = wrap(\Delta\psi - \Delta\phi) \\ \Delta\phi_{res} = \Delta\phi - G\Delta\phi_{suc}; \Delta\phi_{suc} = (G^T G)^{-1}(G^T \Delta\phi) \end{cases} \quad (8)$$

where G denotes design matrix to connect the IFGs and successive interval phase. We substitute the $\Delta\psi_{res}$ and $\Delta\phi_{res}$ into (6) to identify if the network triplets have the unwrapping error. The interferometric triplets owning non-zero K_{amb} are labeled as error-affected triplet. The specific IFG on the triplet is recognized having unwrapping error when the threshold is satisfied,

$$\begin{cases} round[|\Delta\psi_{res}/\kappa|] \geq \varepsilon, \kappa = \pi; \\ round[|\Delta\phi_{res}/\kappa|] \geq \varepsilon, \kappa = 2\pi; \end{cases} \quad (9)$$

where theoretically $\varepsilon = 1$, it can be adjusted because of phase filtering or interferogram multi-looking could also introduce the non-zero K_{amb} value. After the IFGs with ambiguities are detected, the corresponding IFGs are then corrected. The Phase unwrapping error detection and correction are performed iteratively to correct the unwrapping error. The bottom Equation of (8) should not be rank deficient and required the connectivity of the interferometric network. If the condition is not fulfilled, the points with unwrapping errors can be
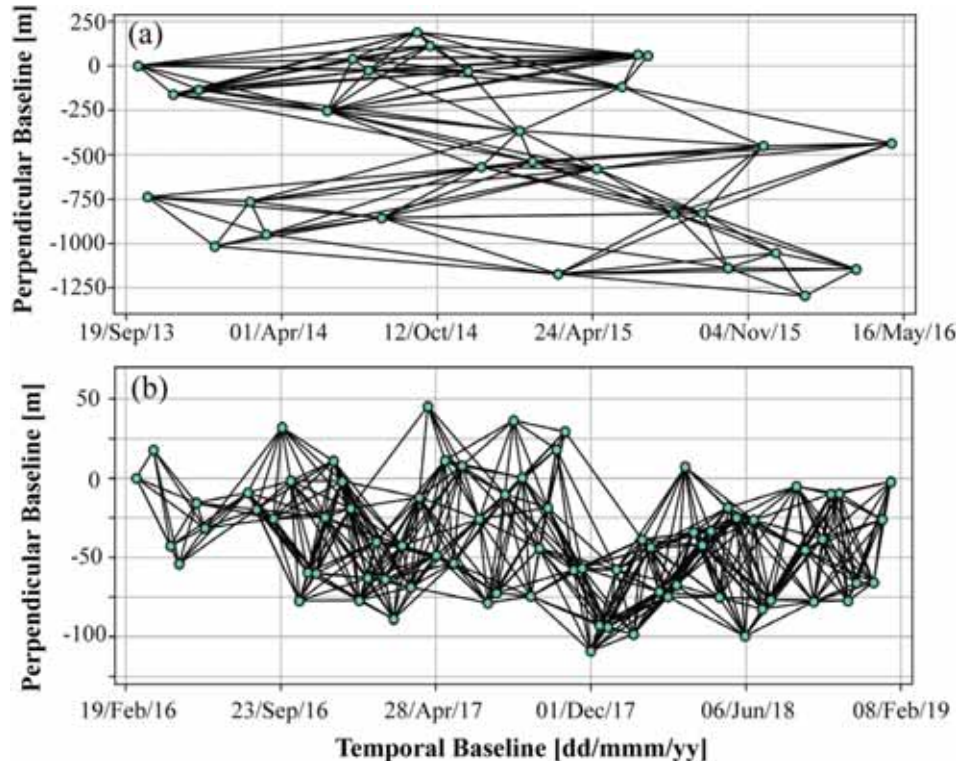

Fig. 12. Spatiotemporal baseline network of (a) CSK and (b) Sentinel-1A datasets.

highlighted in final deformation products. The Phase unwrapping error correction will be verified in Section 4.3.

3.4. Hybrid method

The hybrid method integrates the proposed HgN, SnR, and phase unwrapping error correction strategies in MT-InSAR processing chain. The processing flow is described below,

1) Perform MT-InSAR estimation with the Pixelwise estimator as it not affected by the deformation model error (Wu et al. 2019), to select coherent points and retrieve the unwrapped phase of the redundant arcs which constructed by LFCN.
2) Carry out the discrete search of Δh with Equation (4) among remaining arcs to select arcs with small height difference.
3) Detect isolated sub-networks and carry out network adjustment for each sub-network and select the CPs.
4) Retrieve the unwrapped phase of CPs with Pixelwise estimator and construct the constrained network with DNT.
5) Carry out SnR for each network and estimate the unwrapped phase of all coherent points by network adjustment.
6) Phase unwrapping error correction.
7) Estimate parameters by post-processing.

In Step 3), the distribution of selected CPs is affected by the threshold of the height differences and the arc quality, which will be discussed in Section 4.1. In step 6), multi-looking or phase filtering may result in non-closure phase, affecting the success rate of the unwrapping error

detection and correction. Therefore, attention could be paid to points that have large phase jumps. Step 7) is performed after phase unwrapping. Some unwanted phase components can be eliminated, such as the orbital errors (Zhang et al. 2014), the atmospheric delays (Liang et al. 2018), and the topographic residual error (Liang et al. 2019). The steps in green color in Fig. 5 correspond to the standard steps in MT-InSAR processing for phase unwrapping, whereas the steps proposed are marked in light blue.

4. Validation with simulated data

4.1. Height-guided spatial network

136 interferograms are simulated according to the baseline network of Figure S1 in the Supplementary Material. Phase components related to building height (Fig. 2(b)) and thermal dilation are simulated. Phase noise is simulated using a Gaussian function and the different coherent intervals. It is assumed that no APS and orbital error phase are present in the interferograms. After combining all the different phase components and wrapping them in the range of (-π, π], double differenced phase observations are obtained for a spatial network. Equation (4) is applied to select the CPs for evaluating the HgN strategy.

Fig. 6(a) indicates the selected CPs points, which are marked with black dots and distributed on the bottom of buildings. The selected CPs have small height value (Fig. 6(b)) and can be used to construct the propagation path of the arc solutions. To test the effect of the threshold setting in equation (4), we performed the CPs selection using varied thresholds and the quality of simulated datasets. Fig. 6(c) and (d) give
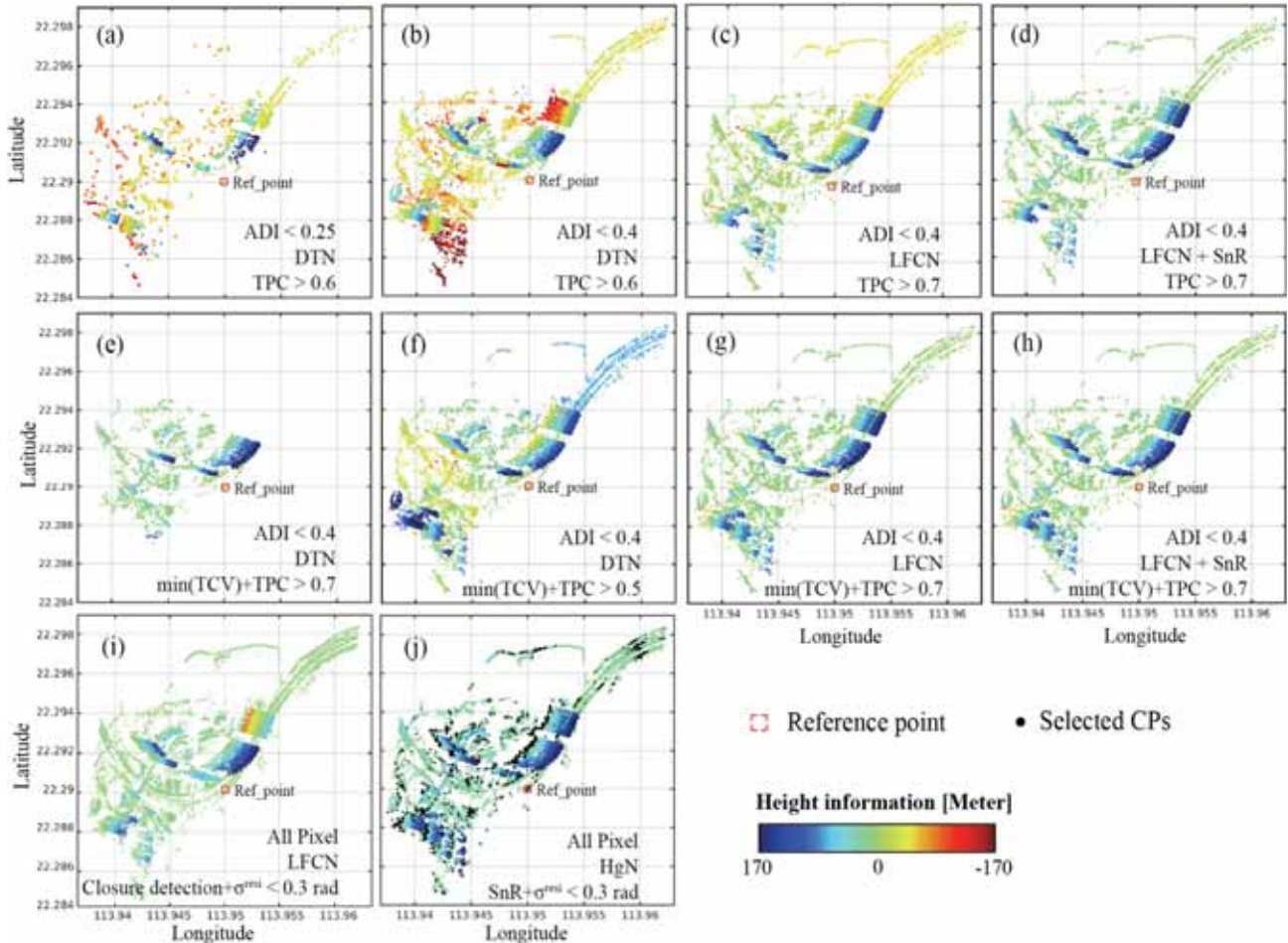

Fig. 13. Height maps estimated by (a-d) PS-InSAR, (e-h) EMCF, (i) Pixelwise estimator, and (j) the proposed method. The red rectangle indicates the location of the reference point. The black dots in (j) are the selected CPs.

two example results of selected CPs with different heights by different height thresholds and simulated datasets, respectively. Fig. 7(a) and (b) show the standard deviation of the estimated height of CPs and the number of generated subnetworks corresponding to different height thresholds and phase quality (i.e., coherence intervals), respectively. The selection of CPs is influenced by the threshold used. When strict threshold and low-quality dataset were used, the subnetworks increased on the building, then the coherent points on the building were selected as the CPs. If the unwrapped phase of CPs is retrieved incorrectly that will affect the effectiveness of the HgN strategy. Therefore, the experience suggests that in general, a moderate height threshold of 60 m can be used to remove the arcs with large height differences, and a TPC threshold of 0.7 is used to ensure the accuracy of parameter calculation, which can be adjusted accordingly.

4.2. Spatial network refinement

Same simulated dataset of Section 4.1 is also used to study the effectiveness of the proposed SnR strategy for spatial network adjustment. Two spatial networks, Delaunay triangular network (DTN) and local freely connected network (LFCN)), are used to construct the double differential observations. After estimating the arc solution, weighted DTN adjustment and LFCN adjustment with phase closure detection (Wu, et al. 2019) are deployed respectively to retrieve the unwrapped phase of the points. As a comparison, we perform SnR before LFCN adjustment to extract the refined network that has the smallest TCV. The accuracy of phase unwrapping is evaluated by calculating the Root Mean Square Error (RMSE) with respect to their simulated "true" values.

Fig. 8 shows some examples of the TCV derived from different spatial networks. The value of TCV (Fig. 8(c)) is reduced notably by the SnR strategy compared to the other networking strategies shown in Fig. 8(a) and (b). In Fig. 9, the results show that network adjustment with SnR has

the smallest RMSE. Compared with the weighted DTN adjustment and the LFCN with phase closure detection, the accuracy of phase unwrapping, i.e., RMSE, is improved by around 0.2 rad along all the simulated datasets with different coherence intervals.

4.3. Correction of unwrapping error

The unwrapped phase is simulated according to the baseline network of Figure S1 in the Supplementary Material. Integer unwrapping errors from π to 6π with random signs are added to some of the observations (about 1 % to 60 % of the observations in the different tests). Gaussian non-closure phase noise is simulated. The unwrapping error detection and correction strategies are applied. The accuracy of the solutions is evaluated by comparing the results with the simulated "true" values. We repeated the experiment with 1000 times to reduce the variability caused by the random errors.

Fig. 10 shows the success rates of error detection are almost 100 % when the unwrapping error of π are added (green line), while the rates are about 93 % (red line) when the unwrapping error added are larger than π. The mean success rates are higher than 96 % (blue line). Fig. 11 shows the success rates of error correction under different percentages of errors added. For the errors added is π, the success rates are very high. For the errors added larger than π, the estimator significantly reduced the number of IFGs with errors to<5 % when the added errors are<30 % of IFGs. When the added errors are>30 %, the estimator only corrects some of them and some new unwrapping errors may potentially be caused by the error correction. The histogram in Fig. 11 shows the percentages of new errors generated when the added ambiguities varied from -4π to 4π. In reality, unwrapping errors are normally moderate in size. Points with large unwrapping errors should have been detected by techniques such as closure detection in the unwrapping process.
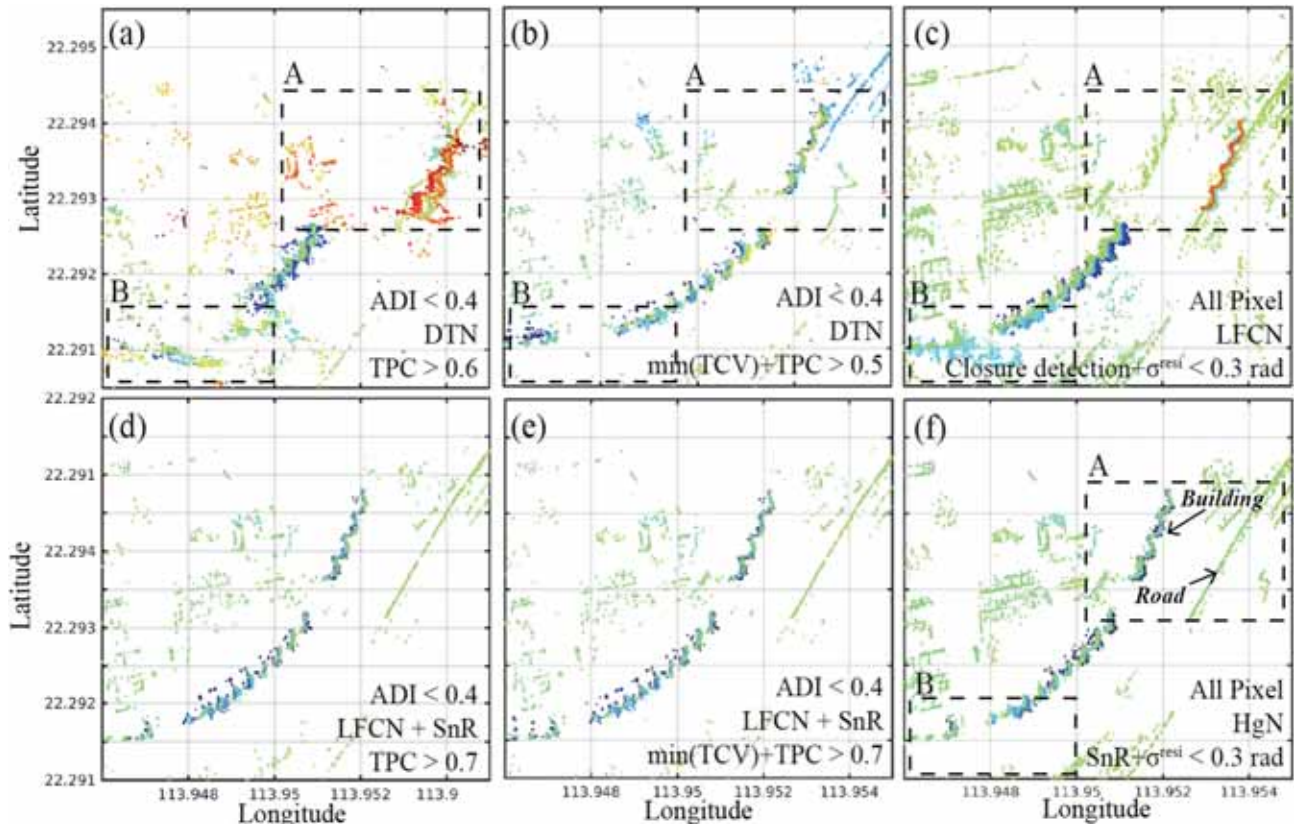

Fig. 14. Distributions of coherent points after geolocation refinement using the height results in (a) Fig. 13-b, (b) Fig. 13-f, (c) Fig. 13-i, (d) Fig. 13-d, (e) Fig. 13-h, and (f) Fig. 13-j. The color scale is the same as that used in Fig. 13.
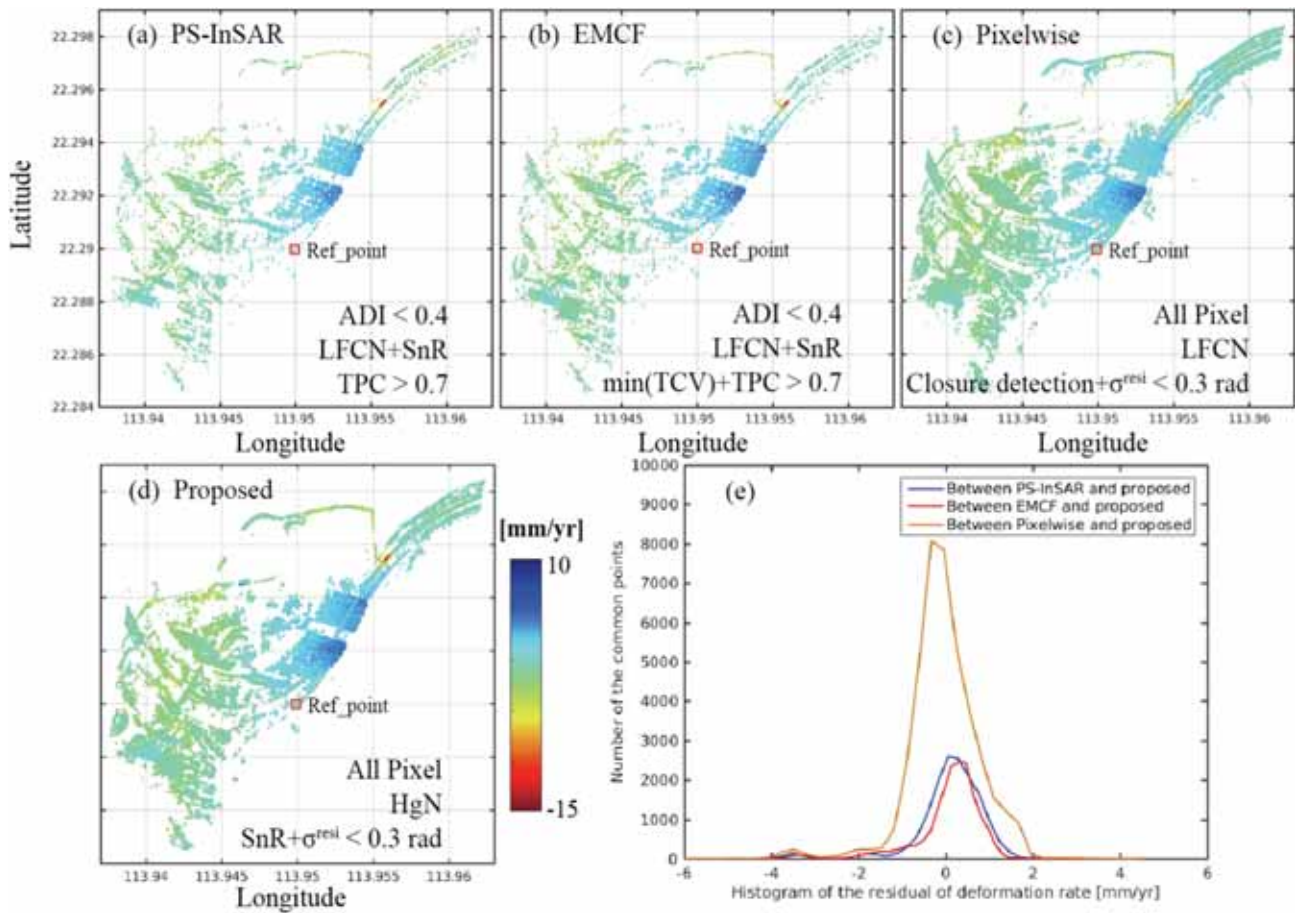
Fig. 15. Deformation rates estimated with (a) PS-InSAR, (b) EMCF, (c) Pixelwise estimator, (d) the proposed method. (e) the histogram of residual between proposed method and other methods.

5. Validation with real data

In this Section, two SAR datasets (COSMO-SkyMed (CSK) and Sentinel-1A) covering Hong Kong urban areas will be used to test the proposed method against the conventional MT-InSAR methods. The scenes covered by CSK are dominated by intersecting buildings and roads in Fig. 2(c). The X-band (3.1 cm) CSK data with large baseline variations make phase unwrapping difficult in such urban areas. The scenes covered by Sentinel-1A are Hong Kong Island with dense high-rise buildings which is used to prove that the proposed method can still improve the solutions when the C-band (5.6 cm) data with stable baselines variation are used. Further information on the SAR datasets is given in Table S1 of the Supplementary Material. Fig. 12 shows the baseline networks of the 136 and 508 interferograms from 30 CSK and 76 Sentinel-1A SAR images, respectively.

5.1. Results from CSK data

The CSK dataset is processed with the proposed method and three current methods, i.e., PS-InSAR (Ferretti et al. 2001), EMCF (Pepe and Lanari 2006), and Pixelwise estimator (Wu et al. 2019). The single master baseline networks for PS-InSAR and multiple master baseline network for EMCF methods are shown in Figure S2 of the Supplementary Material. The Pixelwise estimator and the proposed method used the same baseline network in Fig. 12. The estimated height maps from the CSK data are shown in Fig. 13.

Fig. 13(a)-(d) are the building heights estimated by traditional PS-InSAR method. In Fig. 13(a), only 1,973 PS points are remained based on amplitude dispersion index (ADI) of 0.25. The DTN spatial

networking is constructed for the phase unwrapping. Although the phase quality of the points is high, the solution is still biased, and the building heights cannot be separated from those of the roads. The solution deviates more when points with lower quality are selected (i.e., ADI < 0.4) in Fig. 13(b). In contrast, the LFCN is used to connect the nearest 50 points for each coherent point to generate more redundant observations and the strict threshold (i.e., TPC > 0.7) is used to achieve the results in Fig. 13(c)-(d). In Fig. 13(d), the optimal network is extracted with the SnR strategy for network adjustment and the heights are well estimated. Since the TCV cannot be calculated in single master interferometric network (i.e., PS-InSAR), we used the temporal coherence instead of TCV as the weight in SnR strategy (Jiang and Guarnieri 2020). Fig. 13(e)-(h) are the estimated by EMCF method. Fig. 13(e) is the height maps estimated using DTN spatial network where the minimum cost of TCV is used during the phase unwrapping. The strict thresholds (TPC > 0.7) cause discontinuities in the spatial network so that only limited number of points remain. In Fig. 13(f), a biased height map on the road is achieved when relaxing the threshold to keep more points. In contrast, reliable results are retrieved in Fig. 13(g) and (h) when the LFCN and SnR are applied with the strict thresholds.

The result in Fig. 13(i) retrieved by the Pixelwise estimator is biased by the dense arc solutions with different quality that affected the building height estimation. In contrast, the results estimated by the proposed method shown in Fig. 13(f) indicate that the building heights are well estimated and separated from those of the roads. The solution benefited from the use of the CPs (the black dots) in propagating the arc solution and the SnR in refining the network structure in the network adjustment. The results clearly indicate the effectiveness of the redundant arc observations in maintaining denser points and the necessity of
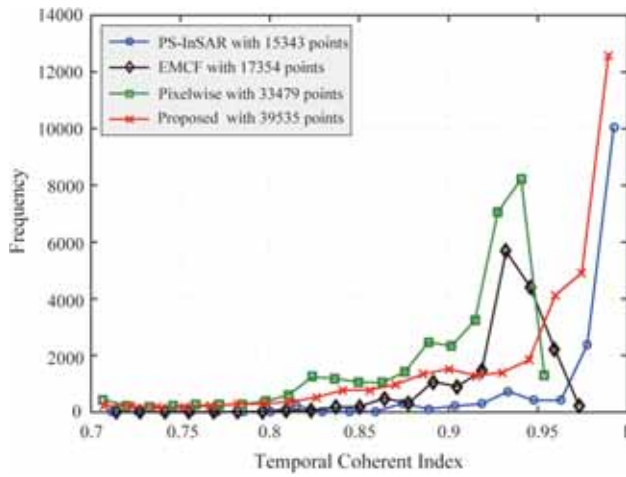
Fig. 16. Histograms of temporal coherence of the unwrapped phase from the different methods.

the SnR strategy in achieving reliable results.

Using the height results in Fig. 13(b), (f) and (i) to refine the geo-locations of the points, the buildings in areas A and B as highlighted by the dashed rectangle are not correctly positioned as shown in Fig. 14(a)-(c), respectively. In contrast, using the height information obtained by using LFCN and SnR in Fig. 13(d), (h), and (j), the points on the buildings are much better aligned. The location of roads and buildings in area A are clearly separated, which is very helpful for urban structural health monitoring. The results of Fig. 14(f) have been overlaid onto the Google Earth map as shown in Fig. 2(c) to demonstrate the excellent quality of the results, the overlaid images for other results have been display in the Figure S4 of the Supplementary Material.

The deformation rates estimated by the different methods are shown in Fig. 15. The results are based on the same unwrapping results as for the height estimation in Fig. 13 (d, h, i, and j). The results show similar deformation patterns although there are some subtle differences as shown in Fig. 15(e), indicating the effectiveness and reliability of the LFCN and SnR strategy. Similar to (Pepe and Lanari 2006), the original and unwrapped IFGs are used to evaluate the accuracy of phase unwrapping using temporal coherence that can be expressed by,

$$\widehat{\gamma} = \frac{1}{M}\left|\sum_{k=1}^{M}\exp\left[j\left(\phi_{wrap}^{k} - \widehat{\varphi}_{unwrap}^{k}\right)\right]\right|, 0 \leq \widehat{\gamma} \leq 1. \tag{9}$$

where ϕ_{wrap}^{k} and $\widehat{\varphi}_{unwrap}^{k}$ are the original wrapped and unwrapped IFG phase, respectively. k is the index of the interferogram used. For a point where $\widehat{\gamma} \rightarrow 1$, it is expected that no unwrapping error is occurred because of the unwrapped phase is nearly perfectly retrieved. The comparison results of the temporal coherence estimated by the results from different methods is shown in Fig. 16. The improvement of the coherence

obtained with the proposed method is evident. Compared with PS-InSAR, EMCF and Pixelwise estimator, the proposed method achieved an improvement of about 158 %, 128 % and 18 %, respectively in terms of the number of points with a temporal coherence value greater than $\widehat{\gamma} = 0.7$. In addition, most points from the proposed method have temporal coherence close to 1, demonstrating the outstanding performance of the proposed method in retrieving the unwrapped phase.

Table 1 shows that the proposed method identified and used 42,310 coherent points and only 670 of them have unwrapping errors with non-closing triplets>10 %, which are significantly reduced compared with the Pixelwise estimator (i.e., 17,527). The EMCF has fewer points (649) with such unwrapping errors, which benefited from the minimum TCV procedure of the network solution. The point density from the EMCF is however much lower.

5.2. Result from Sentinel-1 data

The height information over Hong Kong Island estimated from the C-band Sentinel-1 dataset is shown in Fig. 17. Around 153,000 points in total are obtained and the building heights are clearly separated in Fig. 17(a). Fig. 17(b) shows that only points with lower heights are selected as the CPs to construct the HgN network and to propagate the arc solution during the spatial network integration.

We applied the SnR strategy to refine the spatial network with minimal TCV before the spatial network adjustment. Fig. 18(a) shows the histograms of the TCV of the coherent points. The TCV have been reduced notably after the SnR was used. Fig. 18(b) compares the residual phase between the original and unwrapped phase before and after applying the SnR. The dispersion of phase residuals is significantly reduced, and the standard deviation of the residuals is also reduced from 0.5 to 0.29 rad, indicating the effectiveness of SnR in enhancing the quality of phase unwrapping.

Fig. 19(a) gives an example of phase jumps calculated using the unwrapped phase of the CPs in an interferometric triplet. Fig. 19 (b) and (c) are the estimated deformation rates before and after correcting the phase unwrapping errors. Although similar deformation patterns can be seen in the results, the differential map shows clearly the impact of the unwrapping errors on the estimated deformation rates. The impact of the unwrapping errors on the deformation time series has been presented in the Supplementary Material.

5.3. Computational efficiency

To compare the computational efficiency, we summarized the CPU time in Table 2 for obtaining the results of Fig. 13(d), (h), (i), and (j) from 30 CSK images with an Intel Core-i7-6900 k @3.40 GHz processor. Compared with traditional methods, the proposed method only slightly increases the computation time, and the computational burden is considered affordable in terms of the advantages.

Table 1
Summary of data processing results in Fig. 13.

Slover	IFG network	Initial points (Threshold)	Spatial network	Arc quality	PhU error (>10 %No. of Triplets) without SnR	with SnR	Final points
PS-InSAR Fig. 13(a)	Single-master	1,973 (ADI < 0.25)	DTN	TPC > 0.6	–	–	1,971
PS-InSAR Fig. 13(d)	Single-master	19,668 (ADI < 0.4)	LFCN	TPC > 0.7 & SnR	–	–	15,343
EMCF Fig. 13(h)	Multi-master	19,668 (ADI < 0.4)	LFCN	TPC > 0.7 & SnR	–	649	17,354
Pixelwise Fig. 13(i)	Multi-master	320,000 (all pixels)	LFCN	<0.4 rad & minimum (TCV)	17,527	–	55,057
Proposed Fig. 13(j)	Multi-master	320,000 (all pixels)	LFCN & HgN	<0.4 rad & SnR	–	670	42,310

* **DTN**: Delaunay triangular network; **LFCN**: Local freely connected network; **TCV**: Temporal closure value.
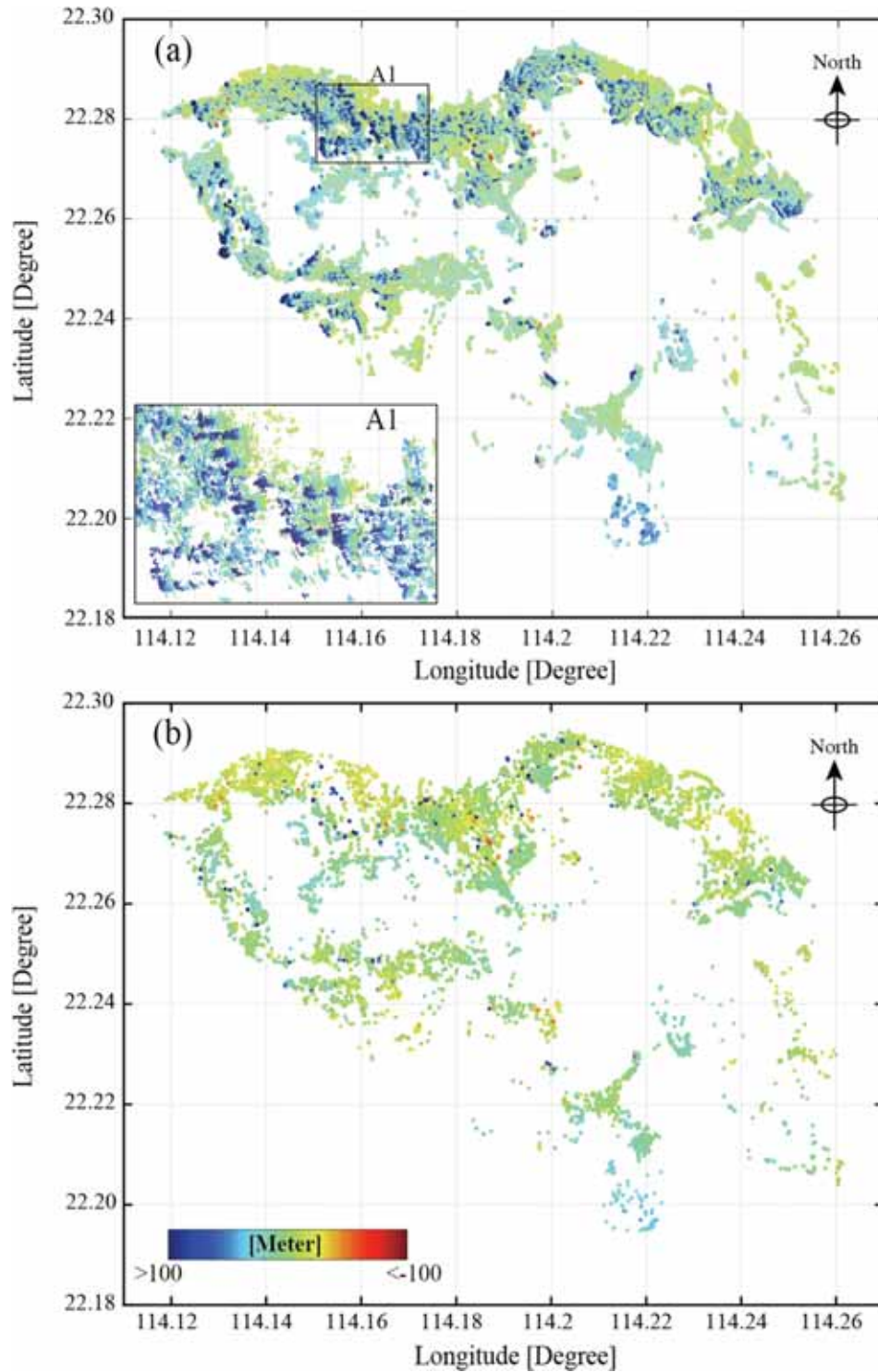
Fig. 17. Estimated heights of (a) all coherent points and (b) selected CPSs. The color indicates the height values that are restricted to range [-100, 100] for better display.

6. Conclusion

We have proposed a hybrid method for MT-InSAR phase unwrapping for applications in urban areas. The height-guided spatial network and two quality control strategies have been proposed to enhance the quality of phase unwrapping to estimate the deformation and building height. Both simulated and real SAR datasets have been used to test the proposed method and compared with the conventional MT-InSAR methods. The simulation experiments indicated that the proposed method can

effectively isolate the propagation paths by identifying the constraint points to overcome the impact of discontinuity of the urban ground infrastructures. The quality of phase unwrapping was enhanced by the network refinement strategy in the reduction of 0.2 rad of RMES. Moreover, the strategy of unwrapping error correction can iteratively identify and correct the phase unwrapping error. In real experiments, the proposed method estimated more accurate building heights and geolocations, which is critical for deformation interpretation in the urban area. In addition, the number of points that be successfully
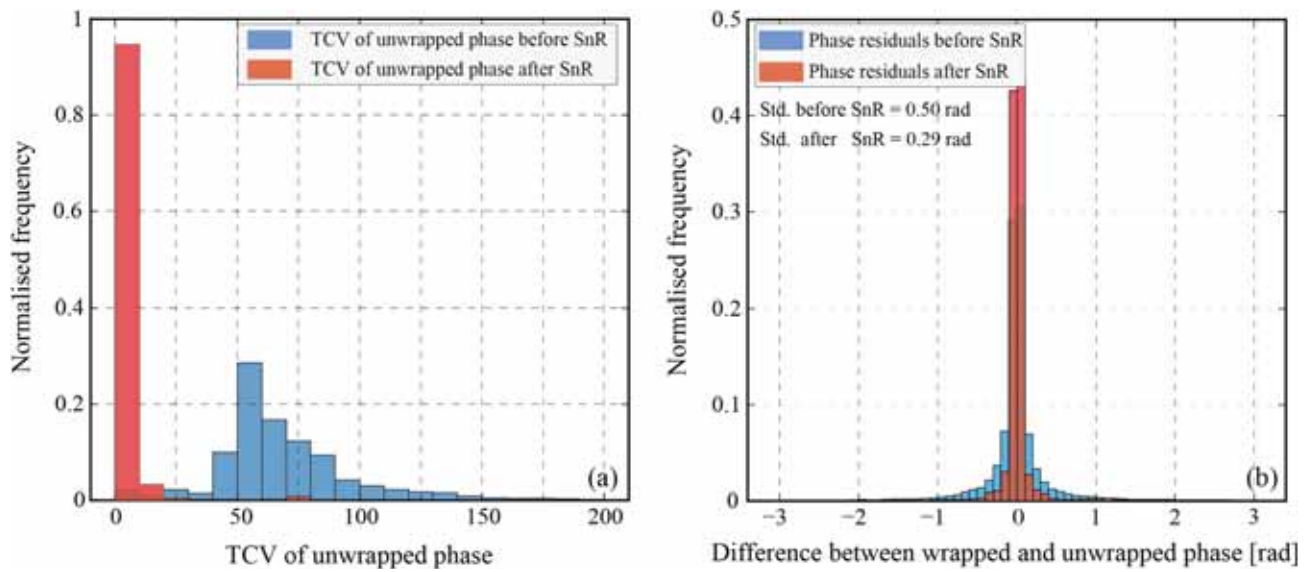
Fig. 18. Histograms of (a) TCV of the unwrapped phase and (b) residual phase of coherent points before and after the SnR.
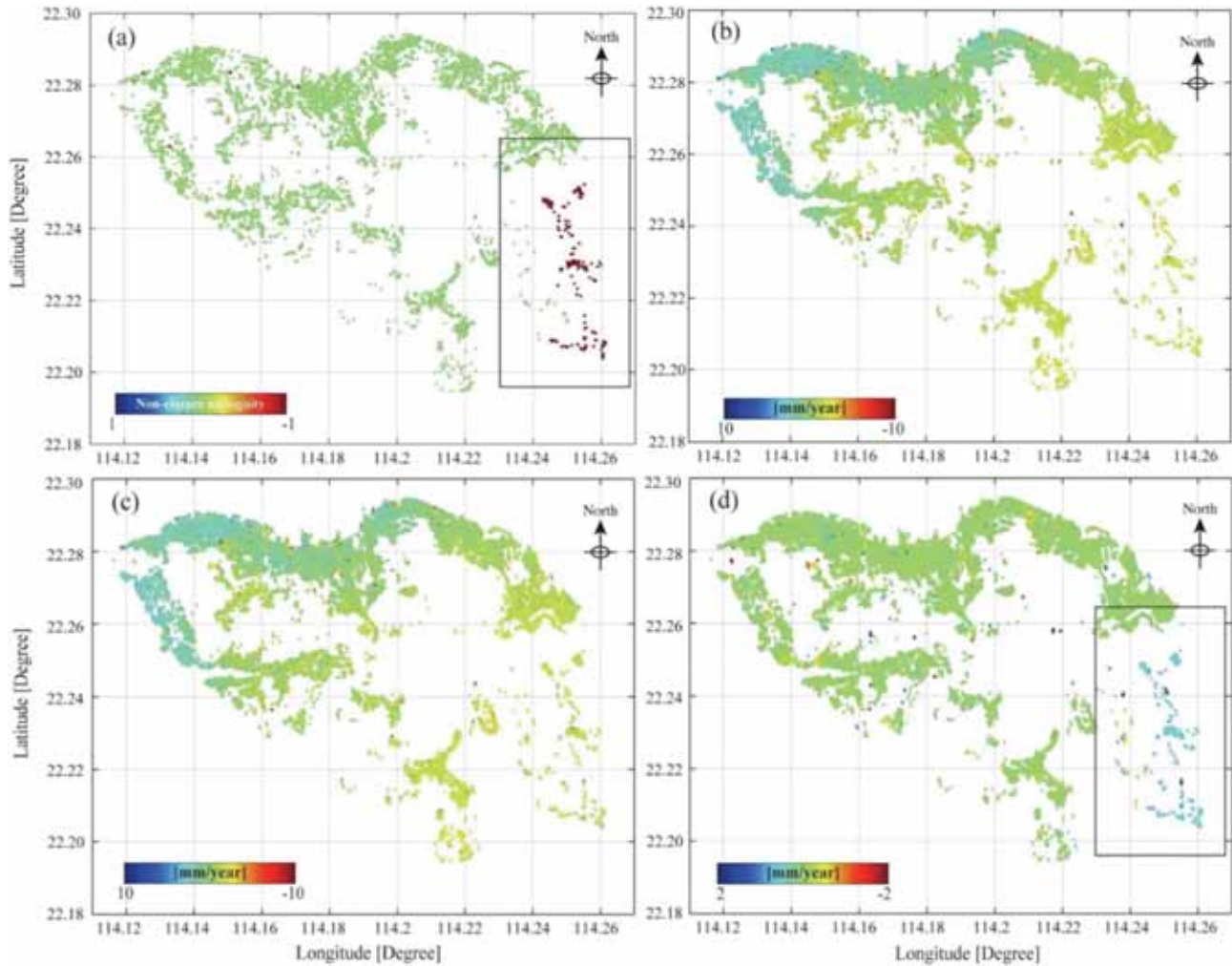

Fig. 19. (a) Unwrapping errors reflected in interferometric triplets calculated from unwrapped phase of the CPs. Deformation rates estimated before (b) and after (c) correcting the phase unwrapping errors. (d) Differential deformation rates between (b) and (c).

Table 2
CPU time of the different methods for processing the CSK dataset (minutes).

Method	Spatial network	Parameter solver Periodogram	LS	Closure phase detection	SnR & error correction	In total
PS-InSAR Fig. 13(d)	LFCN	27	–	–	1	28
EMCF Fig. 13(h)	LFCN	155	–	–	1	156
Pixelwise Fig. 13(i)	LFCN	–	44	6	–	50
Proposed Fig. 13(j)	HgN	50	7	2	3	62

* **LFCN**: Local freely connected network; **HgN**: Heigh-guided network; **LS**: Least-squares.

unwrapped was doubled compared with conventional methods. Each of the proposed strategies in the hybrid method can be individually integrated into the current MT-InSAR data processing framework for urban phase unwrapping.

Declaration of Competing Interest

The authors declare that they have no known competing financial interests or personal relationships that could have appeared to influence the work reported in this paper.

Data availability

Data will be made available on request.

Appendix A. Supplementary data

Supplementary data to this article can be found online at https://doi.org/10.1016/j.jag.2022.102963.

References

Agram, P.S., Simons, M., 2015. A noise model for InSAR time series. J. Geophys. Res. Solid Earth 120 (4), 2752–2771.

Berardino, P., Fornaro, G., Lanari, R., Sansosti, E., 2002. A new algorithm for surface deformation monitoring based on small baseline differential SAR interferograms. IEEE Trans. Geosci. Remote Sens. 40 (11), 2375–2383.

Chang, L., Hanssen, R.F., 2016. A probabilistic approach for InSAR time-series postprocessing. IEEE Trans. Geosci. Remote Sens. 54 (1), 421–430.

Chang, L. (2015). Monitoring civil infrastructure using satellite radar interferometry.

Ferretti, A., Prati, C., Rocca, F., 2001. Permanent scatterers in SAR interferometry. IEEE Trans. Geosci. Remote Sens. 39, 8–20.

Ferretti, A., Fumagalli, A., Novali, F., Prati, C., Rocca, F., Rucci, A., 2011. A new algorithm for processing interferometric data-stacks: SqueeSAR. IEEE Trans. Geosci. Remote Sens. 49 (9), 3460–3470.

Hanssen, R.F., 2001. Radar interferometry: Data interpretation and error analysis. Springer Science & Business Media.

Hooper, A., Zebker, H., Segall, P., Kampes, B., 2004. A new method for measuring deformation on volcanoes and other natural terrains using InSAR persistent scatterers. Geophys. Res. Lett. 31 (23).

Hussain, E., Hooper, A., Wright, T.J., Walters, R.J., Bekaert, D.P.S., 2016. Interseismic strain accumulation across the central North Anatolian Fault from iteratively unwrapped InSAR measurements. J. Geophys. Res. Solid Earth 121 (12), 9000–9019.

Jiang, M.i., Ding, X., Hanssen, R.F., Malhotra, R., Chang, L., 2015. Fast statistically homogeneous pixel selection for covariance matrix estimation for multitemporal InSAR. IEEE Trans. Geosci. Remote Sens. 53 (3), 1213–1224.

Jiang, M.i., Guarnieri, A.M., 2020. Distributed Scatterer Interferometry With the Refinement of Spatiotemporal Coherence. IEEE Trans. Geosci. Remote Sens. 58 (6), 3977–3987.

Jianya, Y.Y.G., 1999. An efficient implementation of shortest path algorithm based on dijkstra algorithm [j]. Journal of Wuhan Technical University of Surveying and Mapping (Wtusm) 3.

Liang, H., Zhang, L., Ding, X., Lu, Z., Li, X., 2018. Toward Mitigating Stratified Tropospheric Delays in Multitemporal InSAR: A Quadtree Aided Joint Model. IEEE Trans. Geosci. Remote Sens. 1–13.

Liang, H., Zhang, L., Lu, Z., Li, X., 2019. Nonparametric Estimation of DEM Error in Multitemporal InSAR. IEEE Trans. Geosci. Remote Sens. 57 (12), 10004–10014.

Ojha, C., Manunta, M., Lanari, R., Pepe, A., 2015. The Constrained-Network Propagation (C-NetP) Technique to Improve SBAS-DInSAR Deformation Time Series Retrieval. IEEE J. Sel. Top. Appl. Earth Obs. Remote Sens. 8 (10), 4910–4921.

Pepe, A., Euillades, L.D., Manunta, M., Lanari, R., 2011. New advances of the extended minimum cost flow phase unwrapping algorithm for SBAS-DInSAR analysis at full spatial resolution. IEEE Trans. Geosci. Remote Sens. 49 (10), 4062–4079.

Pepe, A., Lanari, R., 2006. On the extension of the minimum cost flow algorithm for phase unwrapping of multitemporal differential SAR interferograms. IEEE Trans. Geosci. Remote Sens. 44 (9), 2374–2383.

Qin, X., Li, Q., Ding, X., Xie, L., Wang, C., Liao, M., Zhang, L.u., Zhang, B., Xiong, S., 2021. A structure knowledge-synthetic aperture radar interferometry integration method for high-precision deformation monitoring and risk identification of sea-crossing bridges. Int. J. Appl. Earth Obs. Geoinf. 103, 102476.

Van Leijen, F.J., Hanssen, R.F., 2007. Persistent Scatterer Density Improvement Using Adaptive Deformation Models. IEEE, pp. 2102–2105.

Wang, C., Wang, X.-S., Xu, Y., Zhang, B., Jiang, M.i., Xiong, S., Zhang, Q., Li, W., Li, Q., 2022. A new likelihood function for consistent phase series estimation in distributed scatterer interferometry. IEEE Trans. Geosci. Remote Sens. 60, 1–14.

Wu, S., Zhang, L., Ding, X., Perissin, D., 2019. Pixel-Wise MTInSAR Estimator for Integration of Coherent Point Selection and Unwrapped Phase Vector Recovery. IEEE Trans. Geosci. Remote Sens. 57 (5), 2659–2668.

Wu, S., Yang, Z., Ding, X., Zhang, B., Zhang, L., Lu, Z., 2020. Two Decades of Settlement of Hong Kong International Airport Measured with Multi-Temporal InSAR. Remote Sens. Environ. 248, 111976.

Wu, S., Zhang, B., Liang, H., Wang, C., Ding, X., Zhang, L., 2021. Detecting the Deformation Anomalies Induced by Underground Construction Using Multiplatform MT-InSAR: A Case Study in To Kwa Wan Station, Hong Kong. IEEE J. Sel. Top. Appl. Earth Obs. 14, 9803–9814.

Xiao, R., Jiang, M.i., Li, Z., He, X., 2022. New insights into the 2020 Sardoba dam failure in Uzbekistan from Earth observation. Int. J. Appl. Earth Obs. Geoinf. 107, 102705.

Yang, Y., Pepe, A., Manzo, M., Casu, F., Lanari, R., 2013. A region-growing technique to improve multi-temporal DInSAR interferogram phase unwrapping performance. Remote sensing letters 4 (10), 988–997.

Yu, H., Lan, Y., Yuan, Z., Xu, J., Lee, H., 2019. Phase unwrapping in InSAR: A review. IEEE Geosci. Remote Sens. Mag. 7 (1), 40–58.

Zhang, L., Ding, X., Lu, Z., 2011. Modeling PSInSAR time series without phase unwrapping. IEEE Trans. Geosci. Remote Sens. 49 (1), 547–556.

Zhang, L., Ding, X., Lu, Z., Jung, H.-S., Hu, J., Feng, G., 2014. A novel multitemporal InSAR model for joint estimation of deformation rates and orbital errors. IEEE Trans. Geosci. Remote Sens. 52 (6), 3529–3540.

Zhang, Y., Heresh, F., Falk, A., 2019. Small baseline InSAR time series analysis: Unwrapping error correction and noise reduction. Computers & geosciences, 104331.